Electronic Supplementary Material (ESI) for Dalton Transactions.

Electronic Supplementary Information for

Ligand Effects on the Structure, Mixed-valence Sites and Magnetic Properties of Novel Pentanickel String Complexes

Cheng-Chang Chiu,[a] Gene-Hsiang Lee,[a] Tien-Sung Lin,[a]
and Shie-Ming Peng*[a,b]

[a] Department of Chemistry, National Taiwan University, No. 1, Sec. 4, Roosevelt Rd., 10617 Taipei, Taiwan.
E-mail: smpeng@ntu.edu.tw
[b] Institute of Chemistry, Academia Sinica, 128 Academia Road, Section 2, Nankang, Taipei, Taiwan.

Content

1. Synthetic route of the precursors (**P1** and **P2**), ligands (**L1**–**L4**) and complexes **1**–**8**

The four main ligands H_2Tspnda, H_2Tsphpnda, H_2Mspnda and H_2Msphpnda were synthesized on the basis of palladium-catalyzed Buchwald cross-coupling of halides and amines.[1] Complexes **1** and **2** are synthesized by using H_2Tspnda as ligand; complexes **3** and **4** are synthesized by using H_2Tsphpnda as ligand; Complexes **5** and **6** are synthesized by using H_2Mspnda as ligand and Complexes **7** and **8** are synthesized by using H_2Mspnda as ligand. The detail synthetic routes are described in Scheme S1-S3. The EMAC **1**–**8** were synthesized by the reaction of $Ni(OAc)_2{\cdot}4H_2O$ with ligands at high temperature (220 ^oC) by employing naphthalene as solvent and $[FeCp_2](PF_6)$ as an oxidizing reagent to generate EMAC **1**–**8**. The KPF_6 and $NaCF_3SO_3$ are the anion source to balance the charge of the EMACs. In the course of the reaction, the complexes might generate four different configurations by head-tail counting, which are (4,0), (3,1), (2,2)-*cis* and (2,2)-*trans* forms. Interestingly, the structure prefer to be presented in (2,2)-*trans* forms. It is mainly due to the configuration is more stable and the steric hindrance effect. In addition, we perform the fine-tune H_2Tspnda and H_2Msnda ligands to increase the solubility of the complexes. The solubility of the phenyl-substituted ligands (H_2Tsphpnda and H_2Msphpnda) is obviously better than the H_2Tspnda and H_2Mspnda ligands.

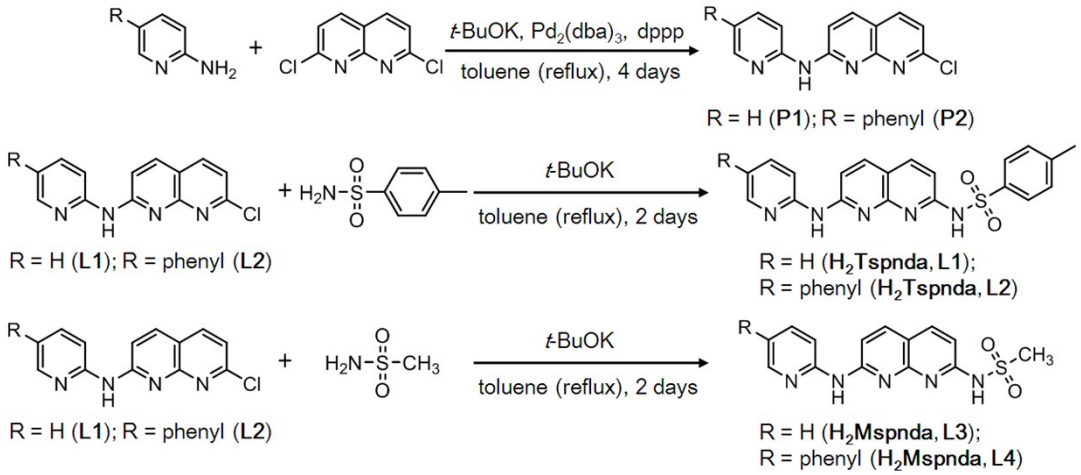

Scheme S1. Synthetic routes of the precursors (**P1** and **P2**) and the ligands (**L1**–**L4**).

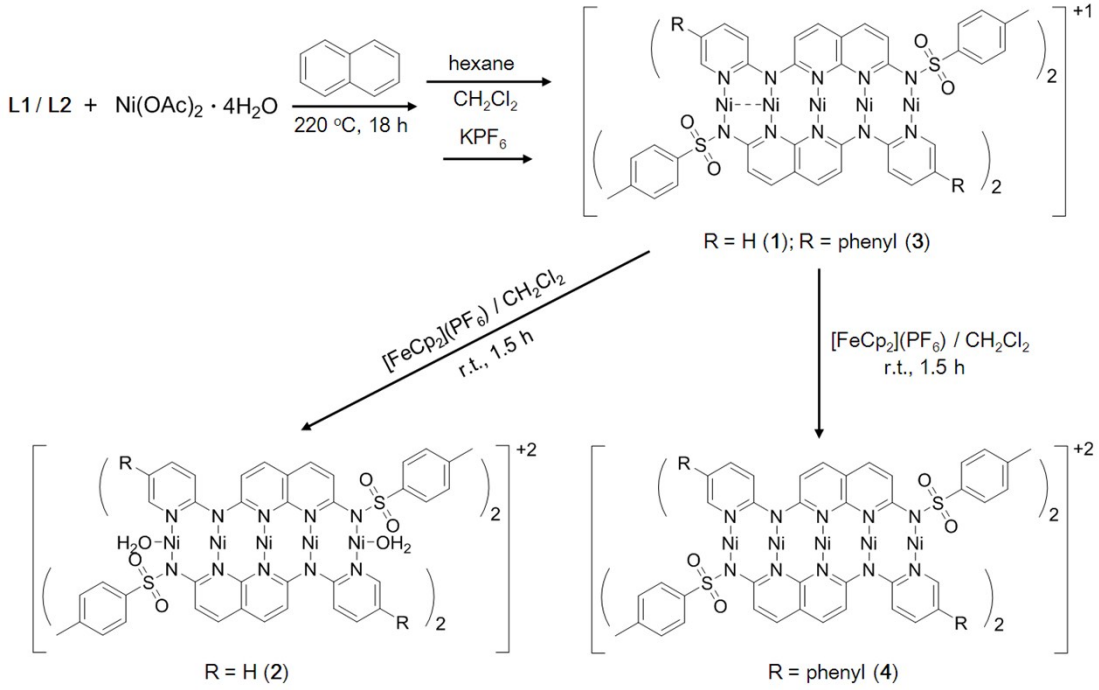

Scheme S2. Synthetic routes of the complexes **1**–**4**.

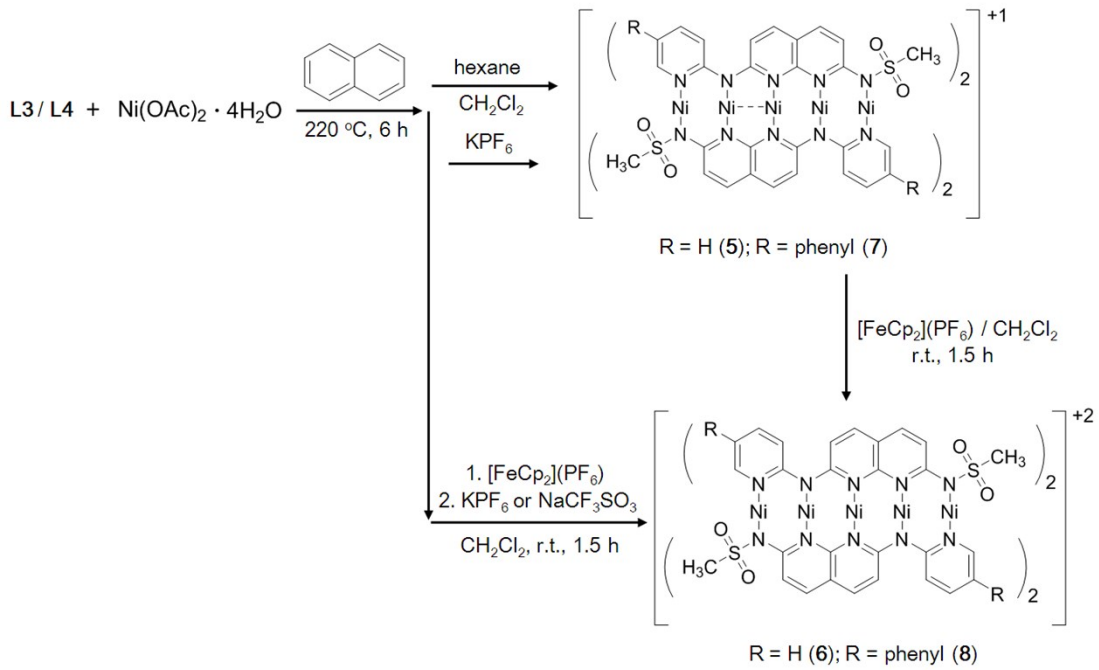

Scheme S3. Synthetic routes of the complexes **5**–**8**.

2. Infrared spectroscopic data of complexes $[Ni_5]^{9+}$ (**1**, **3**, **5** and **7**)

For complexes **1**, **3**, **5** and **7**, the infrared spectra shows that the data were recorded on a Nicolet iS5 Fourier Transform IR spectrometer in the range of 500-4000 cm^{-1} and using KBr pellets, and the PF_6^- anion peaks are detected at around 840 cm^{-1} for these complexes.

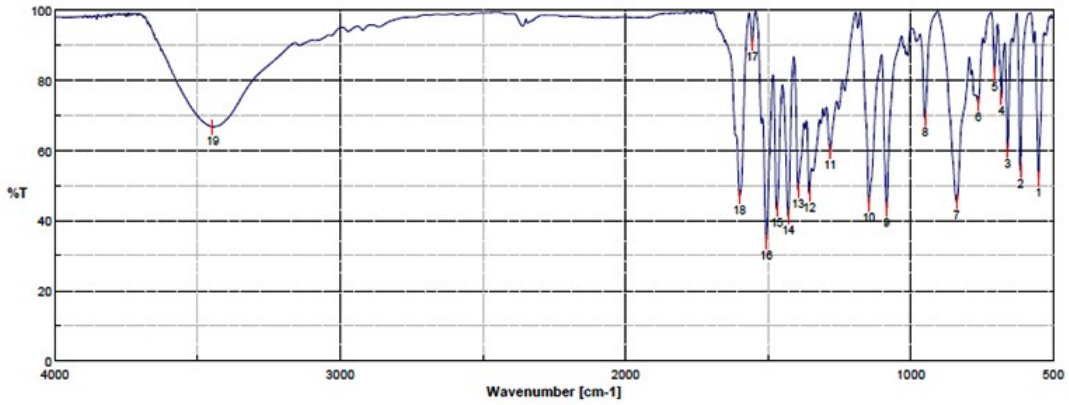

No.	cm-1	%T	No.	cm-1	%T	No.	cm-1	%T	No.	cm-1	%T	No.	cm-1	%T
1	552.506	51.8593	2	617.11	54.347	3	660.982	60.2536	4	682.195	75.0116	5	706.783	82.1301
6	764.155	73.3175	7	839.848	45.2948	8	951.217	69.1698	9	1084.76	43.1417	10	1147.44	44.7544
11	1283.4	59.8342	12	1356.19	47.6878	13	1395.25	48.6793	14	1429.48	41.0769	15	1470.46	43.2671
16	1507.1	34.0747	17	1556.27	90.4396	18	1600.63	46.9132	19	3447.14	66.741			

Figure S1. IR spectroscopic data of complex **1**, the PF_6^- anion peak at 840 cm^{-1}.

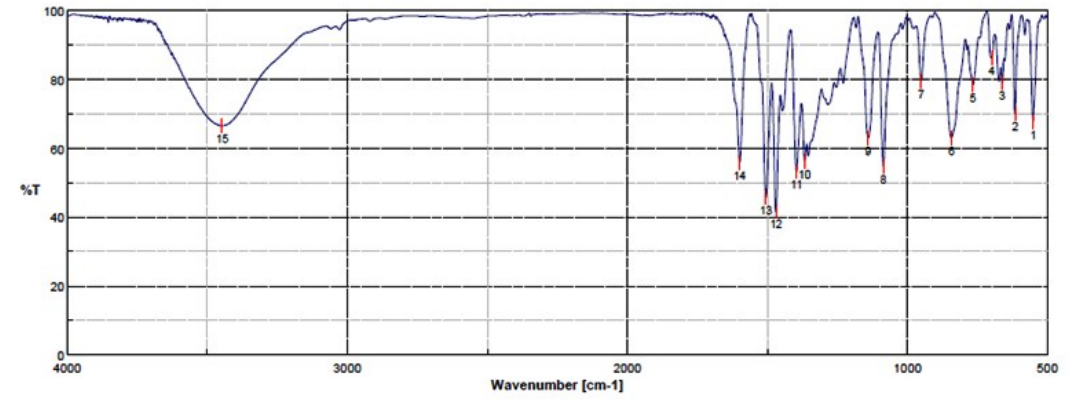

No.	cm-1	%T	No.	cm-1	%T	No.	cm-1	%T	No.	cm-1	%T	No.	cm-1	%T
1	552.024	67.6994	2	617.11	70.2736	3	661.946	79.0218	4	700.034	86.3042	5	766.566	78.4908
6	843.704	63.0863	7	951.699	79.5104	8	1086.21	54.7945	9	1140.69	62.9817	10	1367.28	56.2535
11	1396.69	53.123	12	1470.46	41.6394	13	1506.13	45.6705	14	1599.18	56.0119	15	3447.14	66.4965

Figure S2. IR spectroscopic data of complex **3**, the PF_6^- anion peak at 844 cm^{-1}.

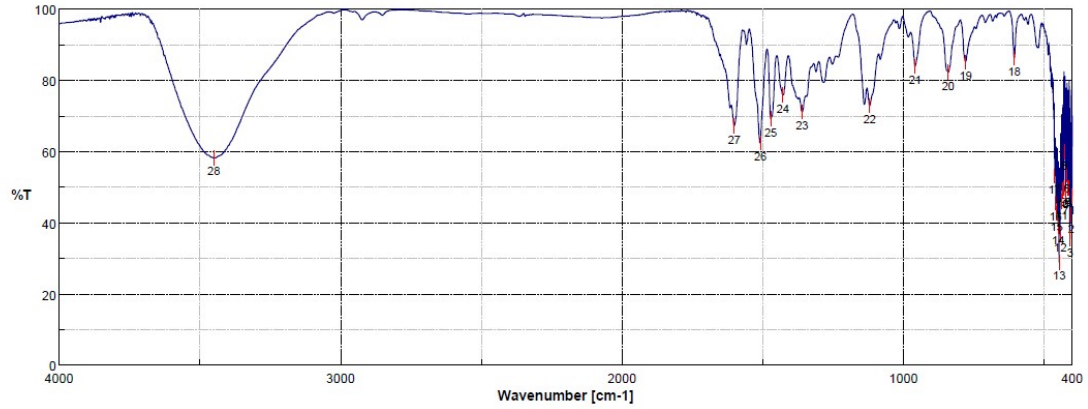

Date/Time 2016/12/6 0:59下午
Operator
File Name NiMspnda(PF6)
Sample Name NiMspnda(PF6)
Comment

No.	cm-1	%T	No.	cm-1	%T	No.	cm-1	%T	No.	cm-1	%T	No.	cm-1	%T
1	401.121	47.5312	2	404.978	42.2459	3	408.835	35.6206	4	412.692	49.8099	5	416.549	49.8276
6	420.406	53.5889	7	424.263	47.5756	8	428.12	59.9941	9	431.977	49.7815	10	435.834	49.2481
11	439.69	46.1338	12	443.547	36.8861	13	447.404	28.9661	14	451.261	39.0696	15	455.118	42.6771
16	458.975	45.5989	17	462.832	53.2325	18	606.503	86.2895	19	779.583	85.2611	20	840.812	82.3578
21	958.93	84.0436	22	1120.44	72.944	23	1360.05	71.2231	24	1428.03	76.0376	25	1471.9	69.2491
26	1509.51	62.5037	27	1601.59	67.2956	28	3450.99	58.3051						

Figure S3. IR spectroscopic data of complex **5**, the PF_6^- anion peak at 841 cm^{-1}.

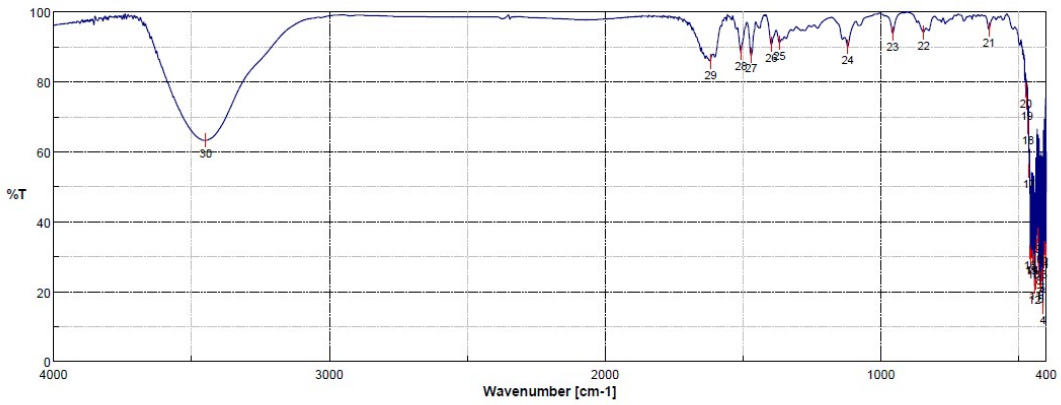

Date/Time 2016/12/6 1:05下午
Operator
File Name NiMsphpnda(PF6)
Sample Name NiMsphpnda(PF6)
Comment

No.	cm-1	%T	No.	cm-1	%T	No.	cm-1	%T	No.	cm-1	%T	No.	cm-1	%T
1	401.121	31.6451	2	404.978	32.501	3	408.835	28.7875	4	412.692	15.6108	5	416.549	25.0894
6	420.406	21.8245	7	424.263	23.7453	8	428.12	26.9824	9	431.977	36.2134	10	435.834	33.1413
11	439.69	22.8201	12	443.547	21.5931	13	447.404	28.6341	14	451.261	29.9695	15	455.118	29.843
16	458.975	31.3647	17	462.832	54.7198	18	466.689	67.3451	19	470.546	74.2169	20	474.403	77.7097
21	608.914	95.0818	22	845.633	94.2627	23	957.002	93.9769	24	1120.44	90.1421	25	1368.25	91.299
26	1397.17	90.82	27	1470.94	87.6319	28	1507.58	88.3766	29	1617.98	85.94	30	3448.1	63.2658

Figure S4. IR spectroscopic data of complex **7**, the PF_6^- anion peak at 846 cm^{-1}.

3. Mass spectrometry for complexes **1**–**8**

MALDI-mass spectra were obtained with a Bruker, New ultrafleXtremet^{TM} for **1**–**8**. The peaks show that the distributions of experiment results are consistent with the simulation data for these four complexes.

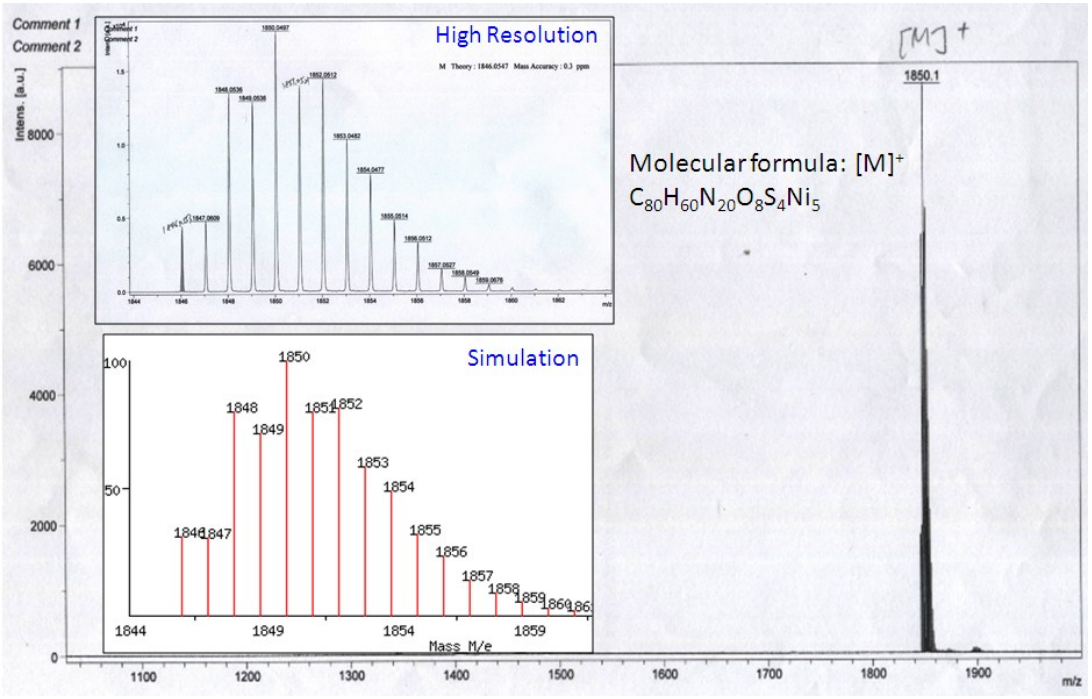

Figure S5. Mass spectrometric data of complex **1**.

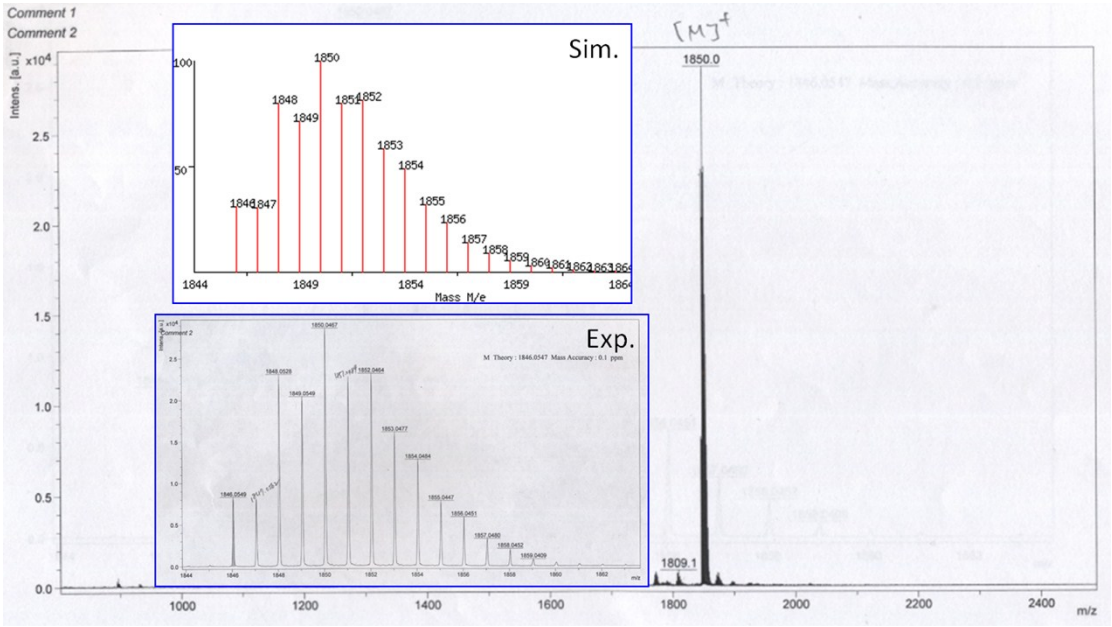

Figure S6. Mass spectrometric data of complex **2**.

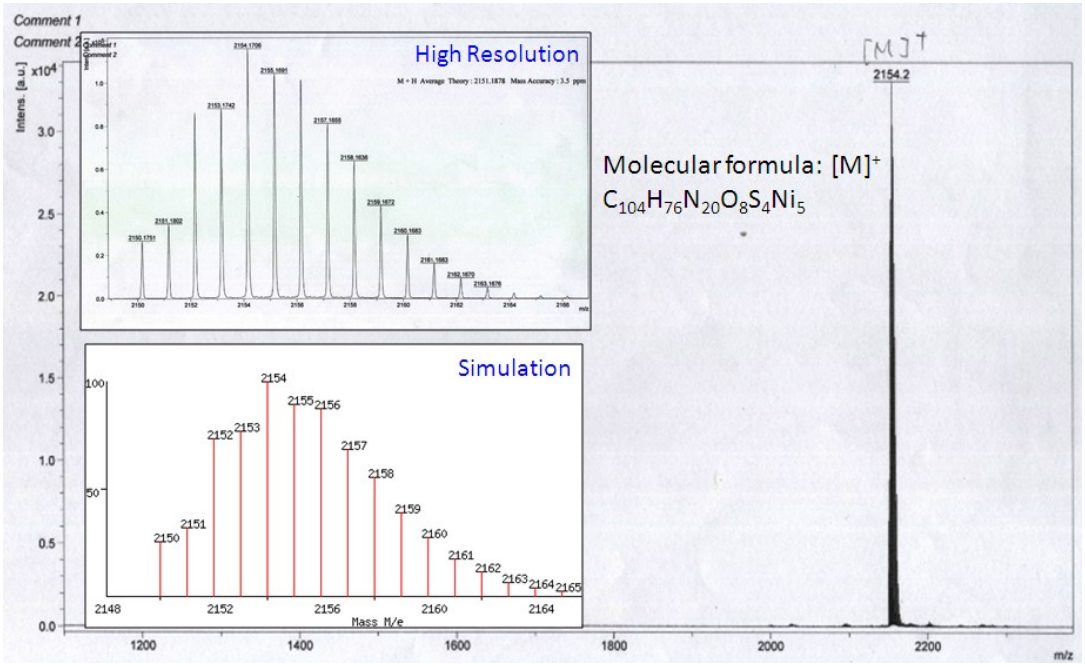

Figure S7. Mass spectrometric data of complex **3**.

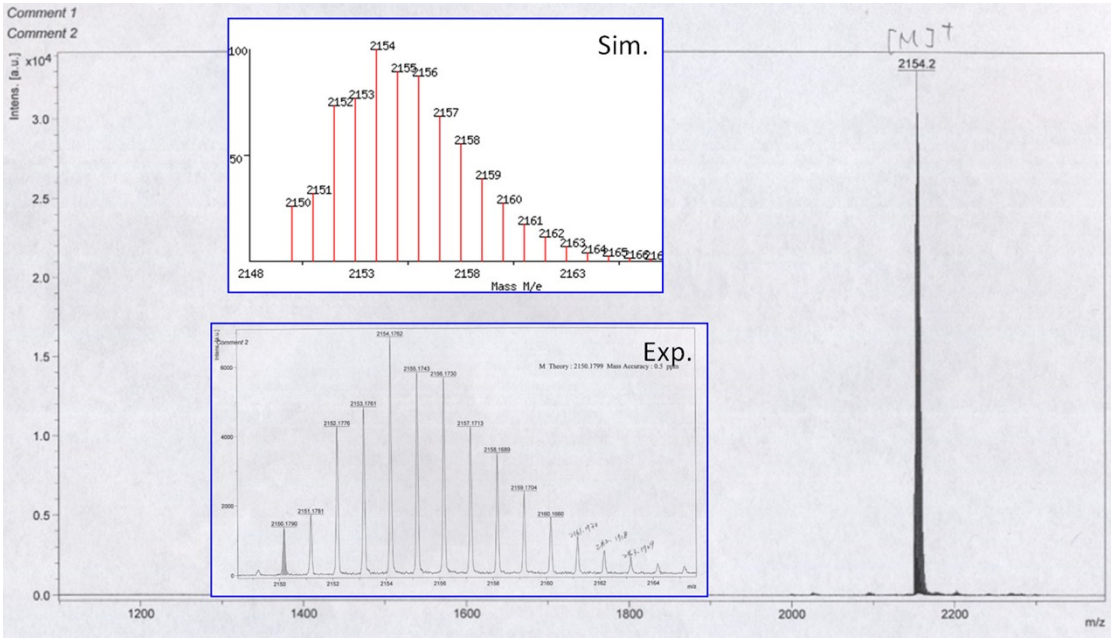

Figure S8. Mass spectrometric data of complex **4**.

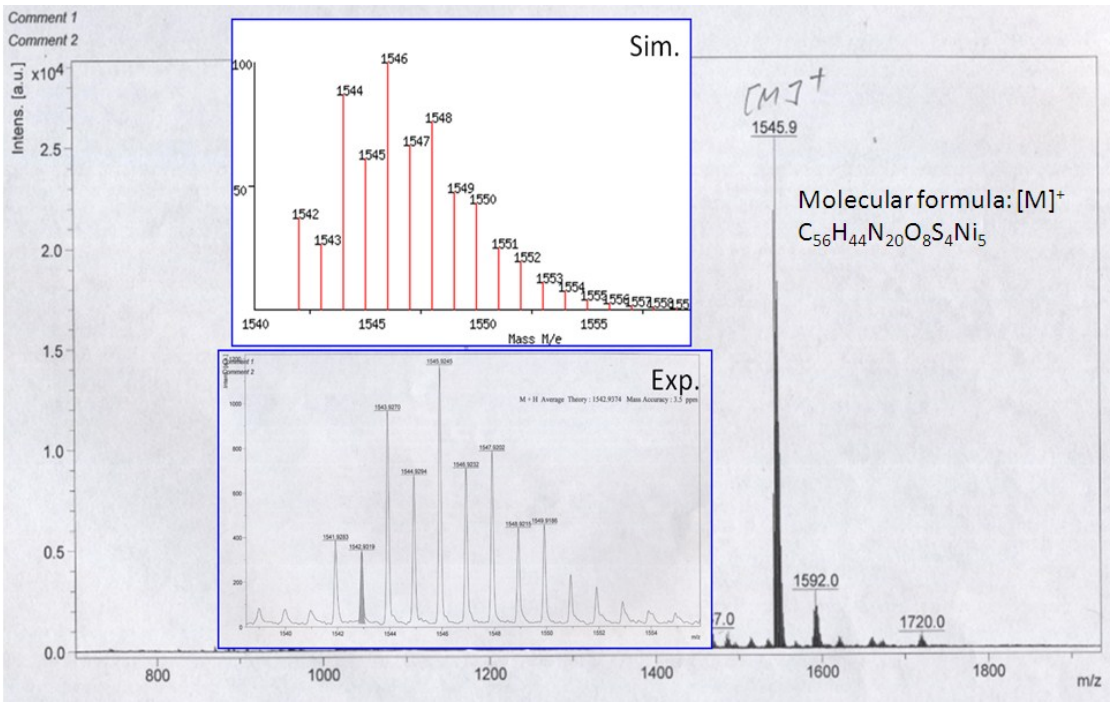

Figure S9. Mass spectrometric data of complex **5**.

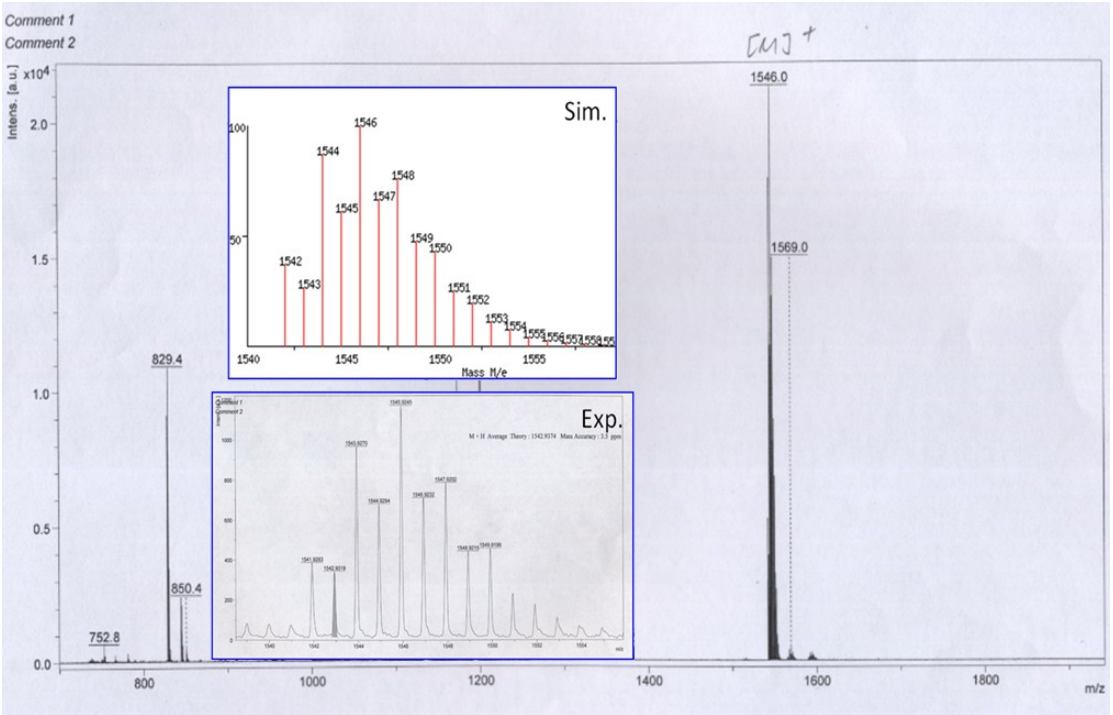

Figure S10. Mass spectrometric data of complex **6**.

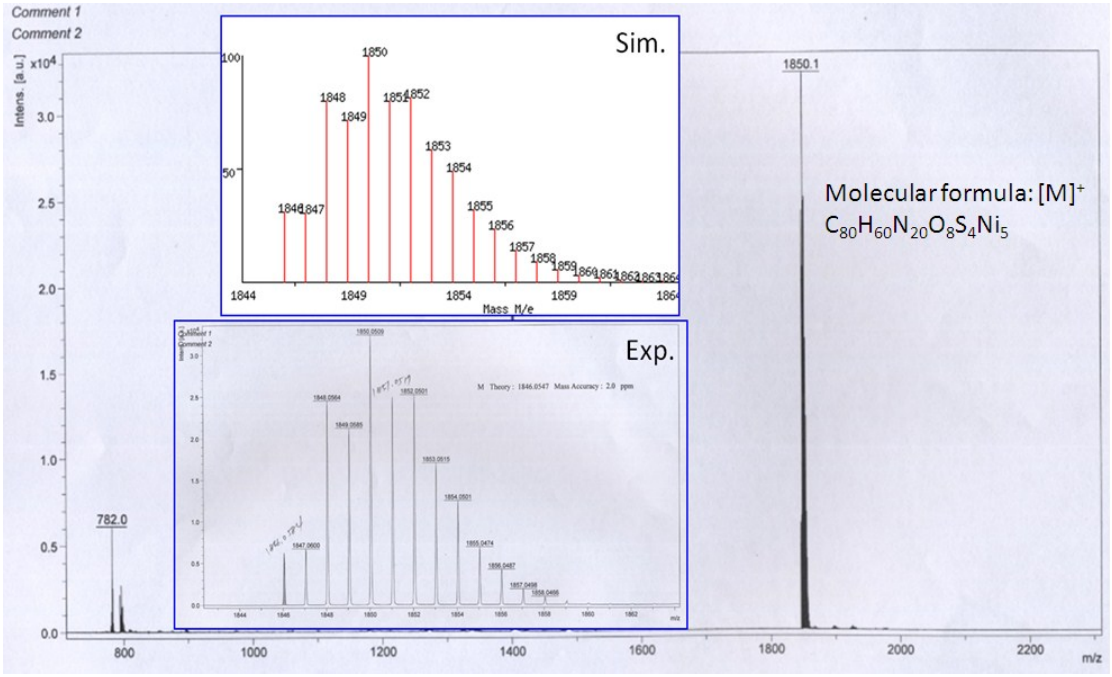

Figure S11. Mass spectrometric data of complex **7**.

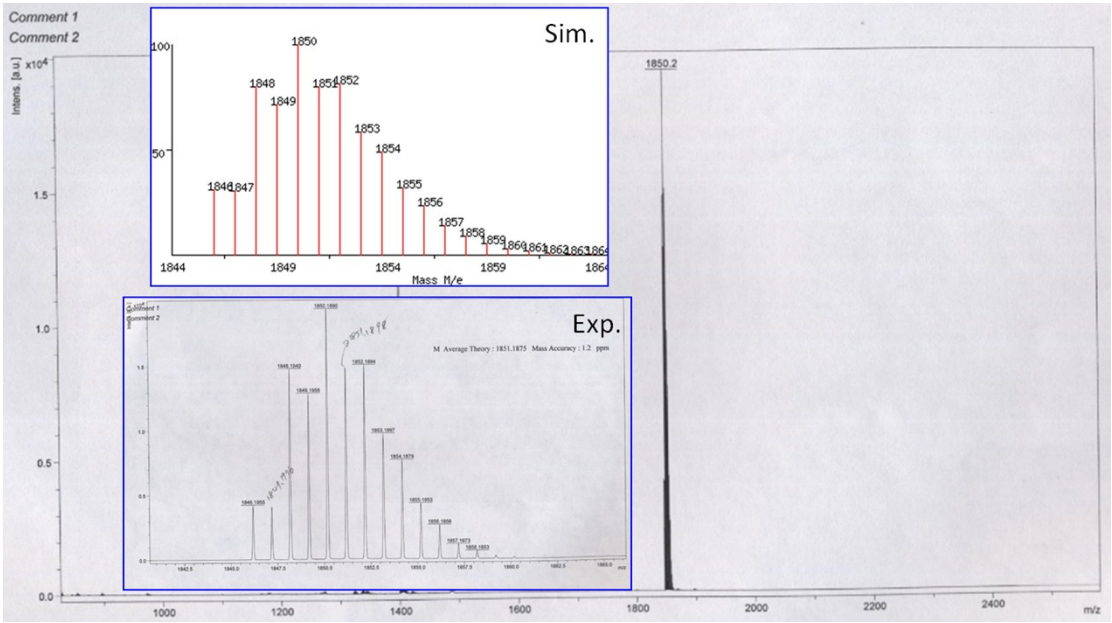

Figure S12. Mass spectrometric data of complex **8.**

4. NMR measurements for complexes **4**, **6** and **8**

^{1}H NMR measurement of **4**, **6** and **8** were recorded in [d_6]-DMSO with a Bruker DPX 400 MHz spectrometer. These complexes show that all of the peaks are shown at low-field, and provide that complexes **4**, **6** and **8** have diamagnetic property.

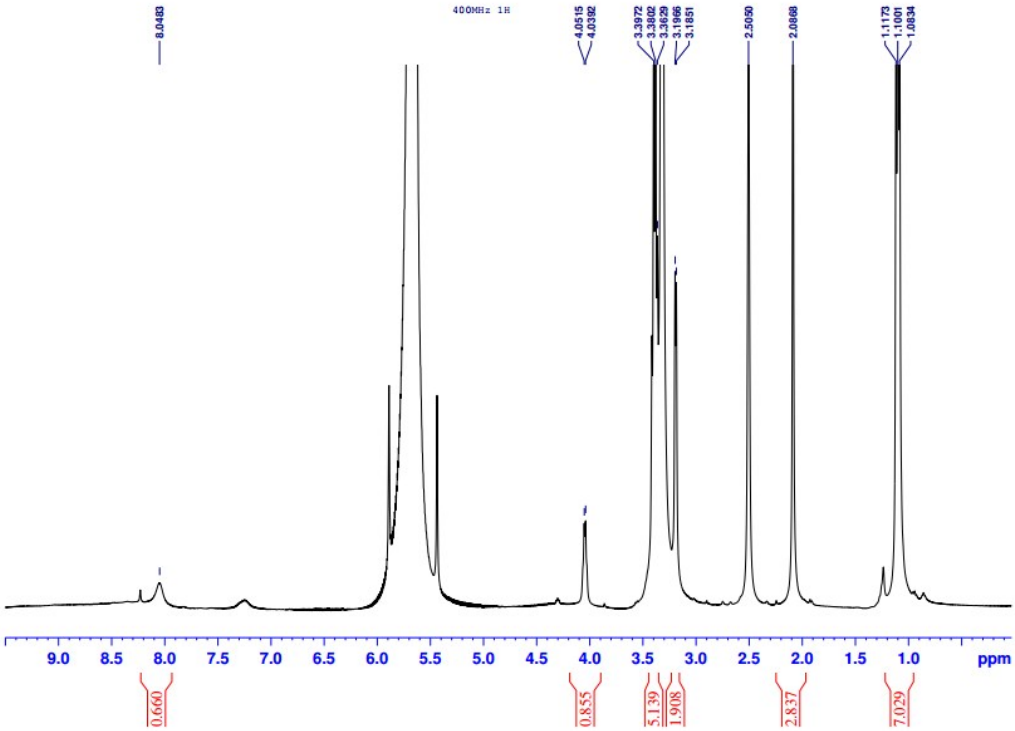

Figure S13. ^{1}H NMR spectrum of complex **4** in [d_6]-DMSO at 400 MHz.

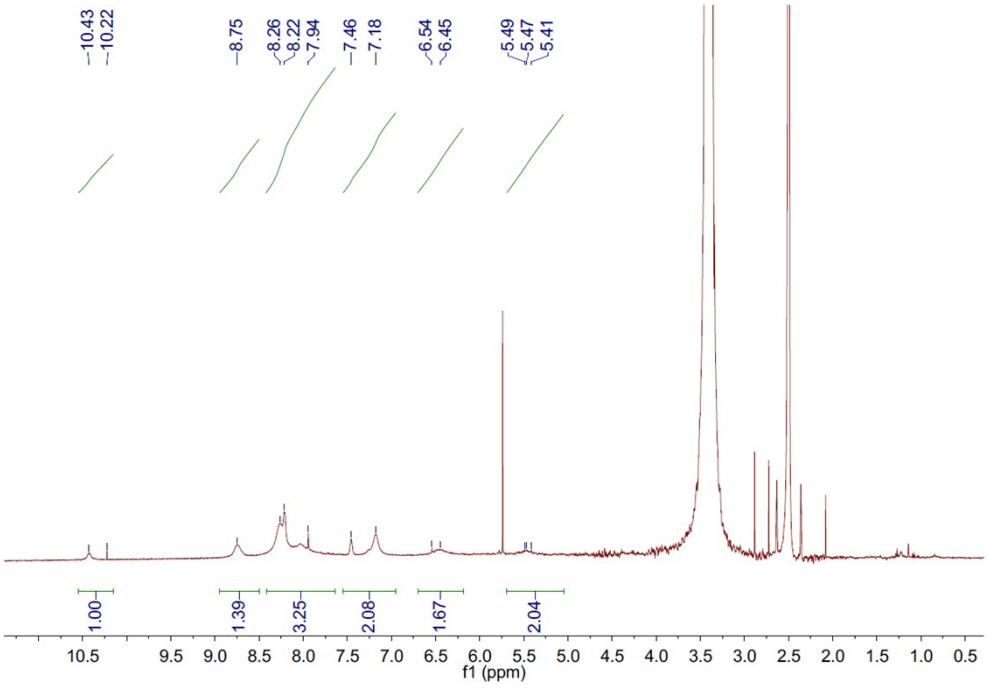

Figure S14. ^{1}H NMR spectrum of complex **6** in [d_6]-DMSO at 400 MHz.

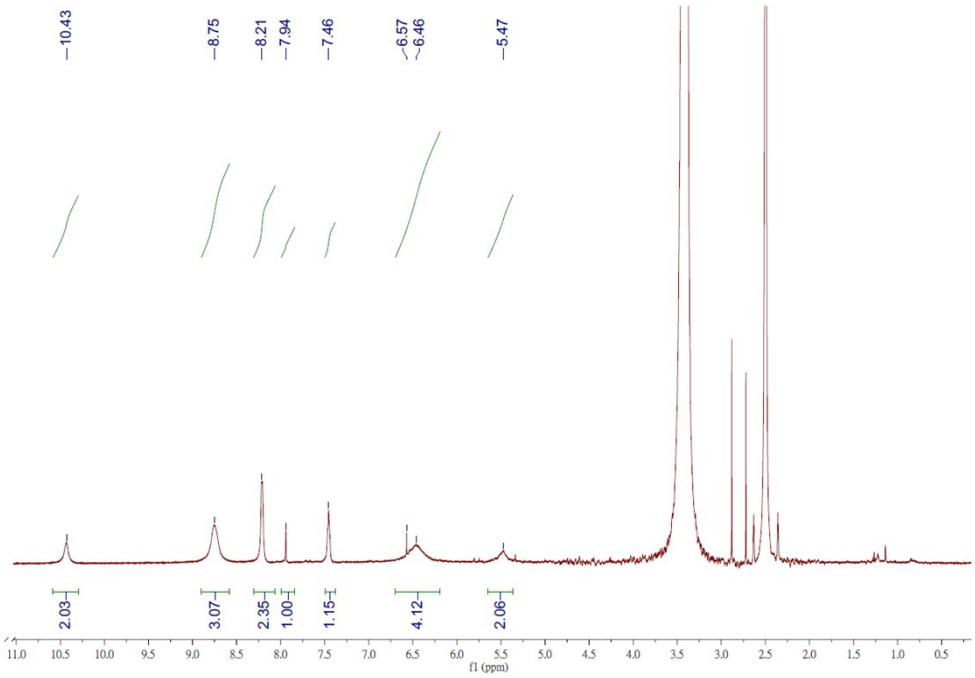

Figure S15. ^{1}H NMR spectrum of complex **8** in [d_6]-DMSO at 400 MHz.

5. UV-Vis and Near-IR spectra

UV-Vis absorption spectra were recorded by a Jasco V-570 spectrometer. There are absorption peaks of d-d transition at around 650 nm for complexes **1**–**4**, and at about 633 nm for **7** and **8**. The signals at around 400nm for these complexes are assigned to the metal-to-ligand charge transfer (MLCT) transition. Complexes **5** and **6** is slightly soluble in DCM, thus, the absorbance is very low when we performed the UV-vis measurement. (see Figure S16-S18).

In addition, we performed the near-IR spectra of complex **1**, **3**, **5** and **7** (see Figure S19, Table S1). The spectra of these four complexes in DMF show two broad bands, one centered at 1431 nm and the other at 1556 nm. These two broad bands are assigned to intervalence charge transfer (IVCT) transition, characteristic of mixed-valence complexes.[2]

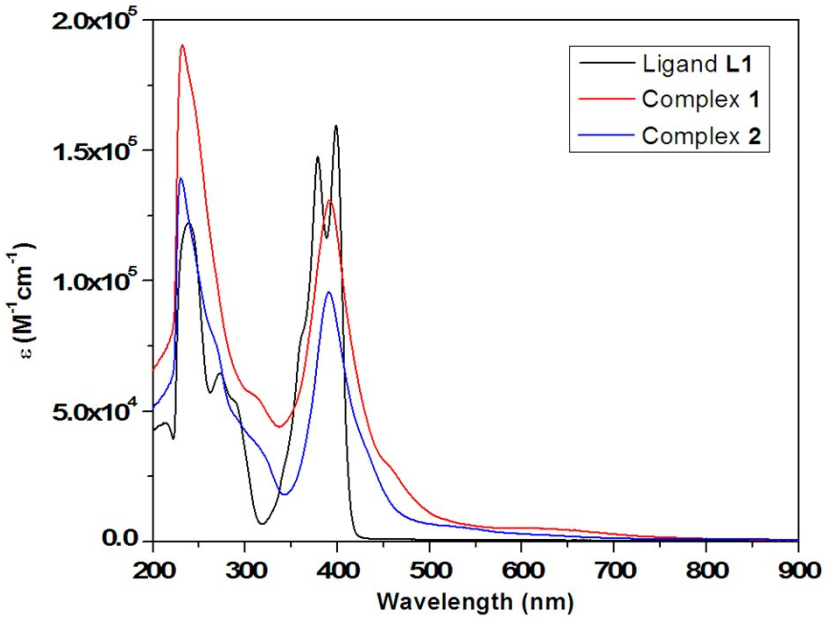

Figure S16. UV-Vis spectra of complexes **1** and **2**, compared with ligand (**L1**) in CH_2Cl_2 (1.5×10^{-5} M).

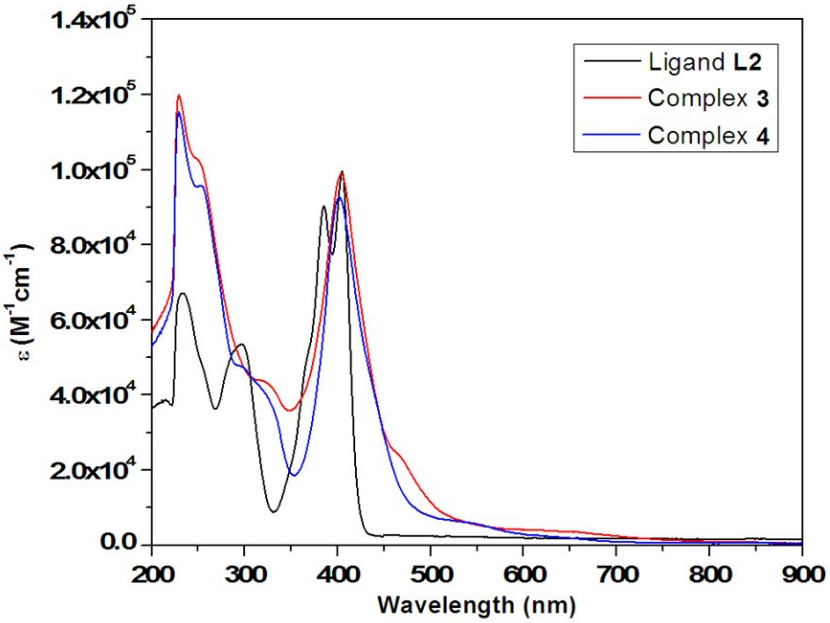

Figure S17. UV-Vis spectra of complexes **3** and **4**, compared with ligand (**L2**) in CH_2Cl_2 (1.5×10^{-5} M).

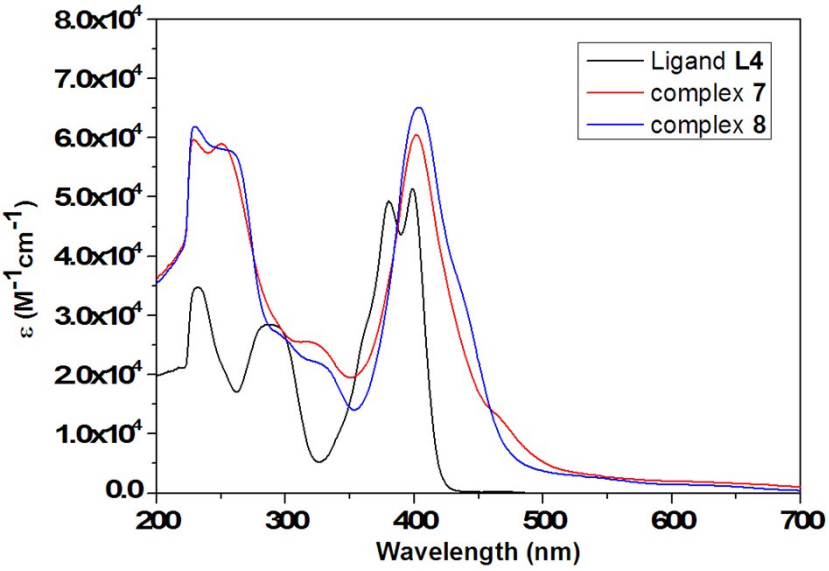

Figure S18. UV-Vis spectra of complexes **7** and **8**, compared with ligand (**L4**) in CH_2Cl_2 (1.5×10^{-5} M).

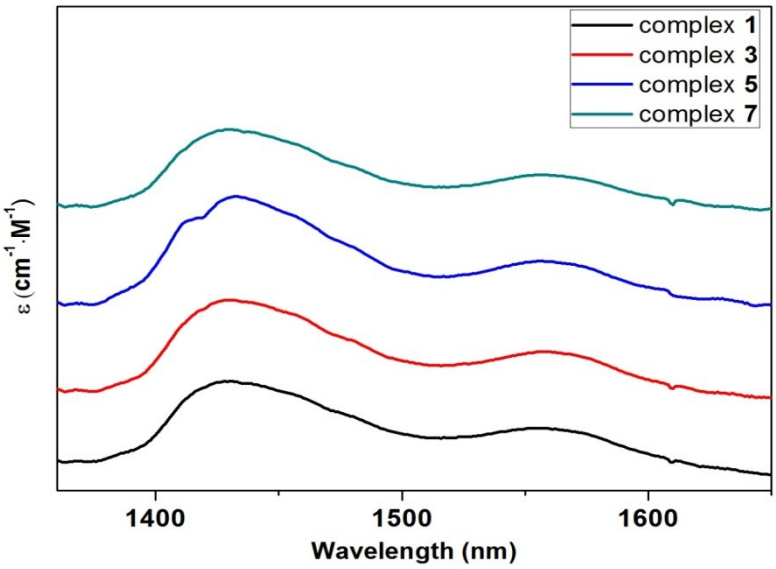

Figure S19. Near-IR spectra of complexes **1**, **3**, **5** and **7** in DMF.

Table S1. Near-IR spectral data for complexes **1**, **3**, **5** and **7**.

Complex	Band 1		Band 2	
(in DMF)	nm	ε (cm^{-1}. M^{-1})	nm	ε (cm^{-1}. M^{-1})
1	1431	1.80×10^3	1556	1.03×10^3
3	1431	1.65×10^3	1556	8.04×10^2
5	1433	1.87×10^3	1556	7.93×10^2
7	1431	1.48×10^3	1556	7.29×10^2

6. Plot of χ_M *vs.T* and μ_{eff} *vs. T* for complexes **1**, **3**, **5** and **7**

Molar magnetic susceptibility data were recorded with a Quantum Design SQUID-VSM system in the range 4-300 K with a 3000 Gauss external magnetic field. The values of μ_{eff} at 300 K, which is close to the value of spin-only ($\mu_{s.o.}$ = 3.87), are 4.10 (for **1**), 4.26 (for **3**), 3.74 (for **5**) and 3.95 μ_{eff} (for **7**) and reveal that these complexes possess an *S* = 3/2 spin configuration.

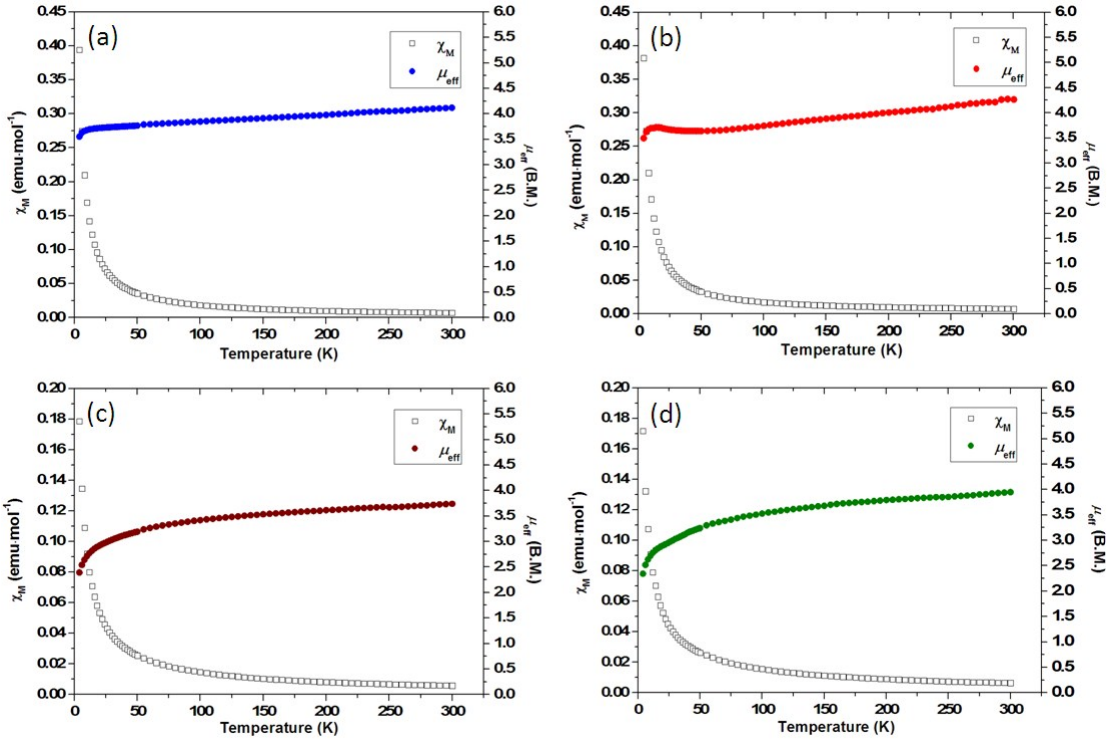

Figure S20. Plot of χ_M *vs. T* and μ_{eff} *vs. T* for (a) **1**, (b) **3**, (c) **5** and (d) **7**.

7. CV measurement for complexes **2**, **4** and **8** in CH_2Cl_2 containing 0.1 M TBAP with a scan rate of 100 $mV \cdot s^{-1}$

Cyclic voltammetry was recorded with a home-made three-electrode cell equipped with a BAS glassy carbon (0.07 cm^2) disk as the working electrode, a platinum wire as the auxiliary electrode, and a home-made Ag/AgCl (saturated) as the reference electrode. There are four reversible redox waves for **2**, **4** and **8**. Complex **6** is slightly soluble in DCM, resulting in the peak is not very clearly when we perform the CV measurement.

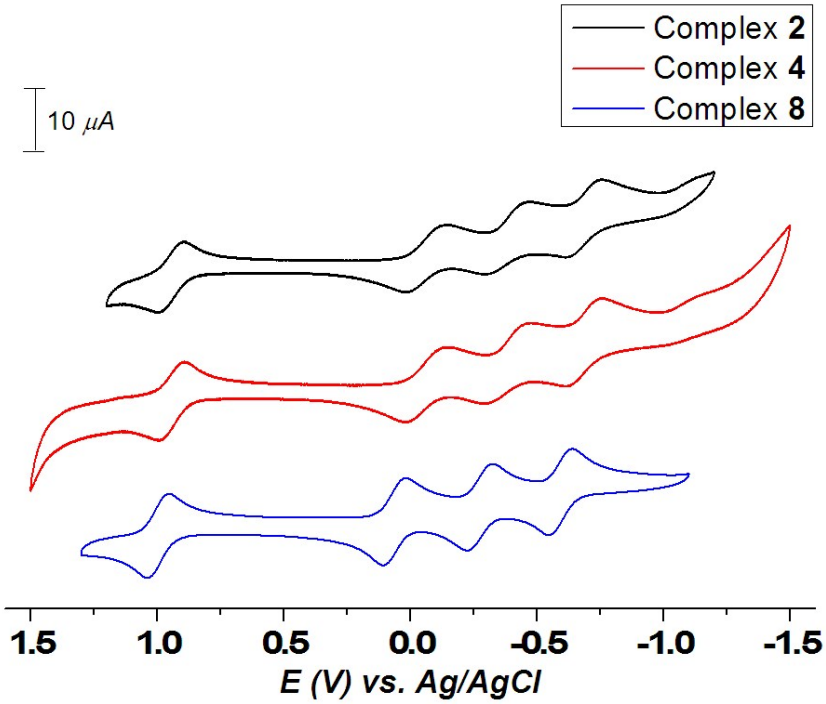

Figure S21. The cyclic voltammograms of **2**, **4** and **8** in CH_2Cl_2 containing 0.1 M TBAP with a scan rate of 100 $mV \cdot s^{-1}$. Top: complex **2**, black line; Middle: complex **4**, red line; Bottom: complex **8**, blue line.

8. EPR spectra for complexes **1**–**3** at 4 K

The EPR measurements of complexes **1**–**3** were performed at 4 K. The best fit spectra parameters of complex **1** are g = 2.03, 2.03 and 2.21 for S = 1/2 and g = 2.09, D = 1.00(1), E = -0.027(2) cm^{-1} for S = 3/2. The parameters of complex **3** are g = 2.02, 2.02, and 2.23 for S = 1/2 and g = 2.09, D = 1.00(1), E = -0.027(2) cm^{-1} for S = 3/2. Note that the D and E values of complexes **1** and **3** are greater than those of **5** and **7** (see main text) which are reasonable in views of the mixed-valence site being localized at the terminal Ni(1)-Ni(2) (relatively asymmetric) in **1** and **3** in comparison with more symmetric Ni(2)-Ni(3) site (with respect to the center of the penta-metal string) in **5** and **7**.

The spectra of **2** exhibits no obvious signals at 4, 10 and 25 K, which shows the ground state is S = 0 and the energy gap between the ground state and the excited state (S = 2) is much greater the thermal energy (J = -13.59 cm^{-1}) for complex **2**.

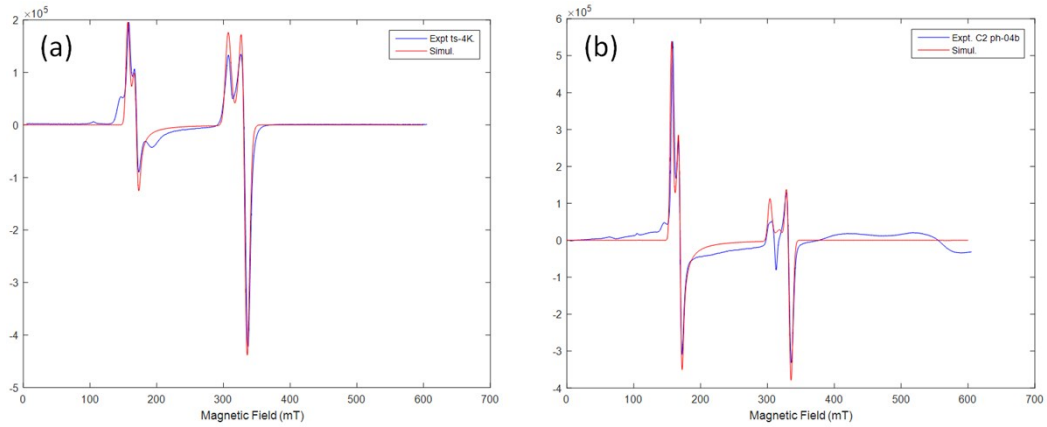

Figure S22. The experimental and simulated EPR spectra at 4 K, (a) complex **1** and (b) complex **3**, experiment (in blue); simulation (in red).

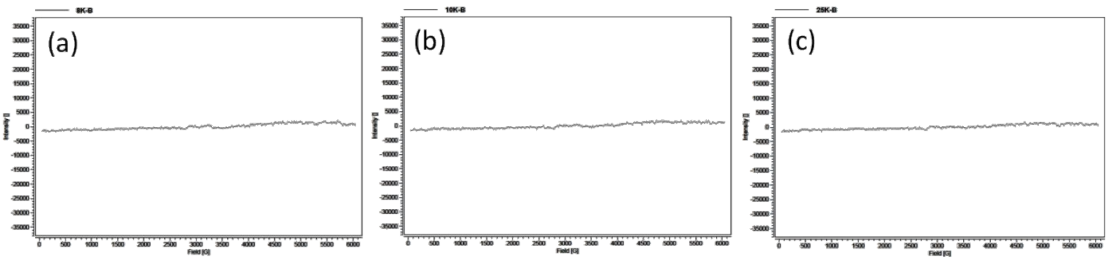

Figure S23. The experimental EPR spectra of complex **2** at (a) 4 K, (b) 10 K

and (c) 25 K, respectively.

9. Crystal data for complexes **1**–**8**

Author's response to the IUCr checkcif file: for complex **5**, Alert level B is due to the DCM solvent disorder. For complex **1**, there exist a disorder between Cl^- ion and PF_6^- anion, whose occupancy are 0.769 (PF_6^-) and 0.231 (Cl^-).

Table S2. Crystal data for complexes **1**–**4**.

	1·2(CH_2Cl_2)(C_3H_7NO)	**2**·3(CH_3OH)	**3**·5.5(CH_2Cl_2)	**4**·8(CH_2Cl_2)
Empirical Formula	$C_{85}H_{71}N_{21}O_9S_4Cl_{4.23}Ni_5P_{0.77}F_{4.61}$	$C_{83}H_{76}N_{20}O_{13}S_4Ni_5P_2F_{12}$	$C_{109.5}H_{87}N_{20}O_8S_4Cl_{11}Ni_5PF_6$	$C_{112}H_{92}N_{20}O_8S_4Cl_{16}Ni_5P_2F_{12}$
Formula weight	2213.85	2273.27	2767.70	3124.96
Crystal color	light-brown	red-brown	light-brown	red-brown
Crystal system	Monoclinic	Tetragonal	Triclinic	Triclinic
Space group	$P2_1/c$	$I4_1/acd$	P-1	P-1
a [Å]	18.1215(7)	27.2637(6)	16.4220(7)	14.6531(5)
b [Å]	17.4460(6)	27.2637(6)	16.8719(8)	18.6083(6)
c [Å]	31.4395(11)	50.6630(10)	22.4552(10)	23.8981(6)
α [°]	90	90	73.6370(14)	86.3807(10)
β [°]	98.5260(10)	90	76.3465(16)	88.3058(10)
γ [°]	90	90	76.0990(18)	71.2244(11)
V [Å]	9829.7(6)	37658.3(18)	5699.4(4)	6156.9(3)
Z	4	16	2	2
T [K]	150(2)	150(2)	150(2)	150(2)
ρ_{calcd} [Mgm^{-3}]	1.496	1.595	1.613	1.686
$R1$[a]/$wR2$[b] [$I > 2\sigma(I)$]	0.0580, 0.1575	0.0551, 0.1487	0.0696, 0.1867	0.0535, 0.1314
$R1$[a]/$wR2$[b] (all data)	0.0742, 0.1766	0.0787, 0.1640	0.0927, 0.2046	0.0682, 0.1440
GOF	1.027	1.045	1.034	1.017

[a] $R1 = \Sigma||F_o|-|F_c||/\Sigma|F_o|$. [b] $wR2 = [\Sigma[w(F^2_o-F^2_c)^2]/\Sigma[w(F^2_o)^2]]^{1/2}$, in which $w = 1/\sigma^2(F^2_o)+(aP)^2+bP$, $P = (F^2_o+2F^2_c)/3$.

Table S3. Crystal data for complexes **5**–**8**.

	5·3(CH_2Cl_2)·2(C_3H_7NO)	**6**·(CH_2Cl_2)	**7**·5.5($C_2H_4Cl_2$)	**8**·6(CH_2Cl_2)
Empirical Formula	$C_{65}H_{64}Cl_6F_6N_{22}Ni_5O_{10}PS_4$	$C_{59}H_{46}Cl_2F_6N_{20}Ni_5O_{14}S_6$	$C_{91}H_{83}Cl_8F_6N_{20}Ni_5O_8PS_4$	$C_{86}H_{72}Cl_{12}F_{12}N_{20}Ni_5O_8P_2S_4$
Formula weight	2089.84	1929.97	2435.13	2650.76
Crystal color	light-brown	red-brown	light-brown	red-brown
Crystal system	Triclinic	Monoclinic	Monoclinic	Monoclinic
Space group	*P*-1	*C*2/c	$P2_1$/n	*C*2/c
a [Å]	14.1494(4)	25.0742(9)	16.2704(5)	32.1417(7)
b [Å]	17.0242(6)	14.4767(6)	37.9133(11)	13.4697(3)
c [Å]	17.9497(6)	18.9389(7)	16.4754(5)	23.6404(5)
α [°]	76.2023(16)	90	90	90
β [°]	72.4156(14)	90.625(2)	104.9136(8)	96.7840(6)
γ [°]	78.5677(14)	90	90	90
V [Å]	3965.4(2)	6874.3(5)	9820.7(5)	10163.2(4)
Z	2	4	4	4
T [K]	150(2)	150(2)	150(2)	150(2)
ρ_{calcd} [Mgm^{-3}]	1.750	1.865	1.647	1.677
$R1^{[a]}/wR2^{[b]}$ [$I>2\sigma(I)$]	0.0879/ 0.2646	0.1066/ 0.2990	0.0713/ 0.1545	0.0690 / 0.1898
$R1^{[a]}/wR2^{[b]}$ (all data)	0.1013/ 0.2859	0.1452/ 0.3373	0.1095/ 0.1717	0.0930/ 0.2188
GOF	1.036	1.206	1.068	1.047

[a] $R1 = \Sigma|F_o|-|F_c|/\Sigma|F_o|$. [b] $wR2 = [\Sigma[w(F^2_o-F^2_c)^2]/\Sigma[w(F^2_o)^2]]^{1/2}$, in which $w = 1/\sigma^2(F^2_o)+(aP)^2+bP$, $P = (F^2_o+2F^2_c)/3$.

Reference

1. S. Wagan and S. L. Buchwald, *J. Org. Chem.*, 1996, **61**, 7240-7241.
2. Mixed Valence Compounds, ed. D. M. Brown, D. Reidel, Dordrecht, Holland, 1980.